Available online at www.sciencedirect.com
SCIENCE DIRECT
Journal of Photochemistry and Photobiology A: Chemistry 182 (2006) 121–127
Journal of Photochemistry and Photobiology A:Chemistry
www.elsevier.com/locate/jphotochem

Preparation and photocatalytic activity of mesoporous anatase TiO_2 nanofibers by a hydrothermal method

Jiaguo Yu *, Huogen Yu, Bei Cheng, Xiujian Zhao, Qingjie Zhang

State Key Laboratory of Advanced Technology for Material Synthesis and Processing, Wuhan University of Technology, Wuhan 430070, PR China

Received 13 August 2005; received in revised form 7 January 2006; accepted 31 January 2006
Available online 6 March 2006

Abstract

Mesoporous anatase TiO_2 nanofibers were prepared by a simple hydrothermal post-treatment of titanate nanotubes. The as-prepared samples were characterized with transmission electron microscopy (TEM), thermogravimetry (TG), X-ray diffraction (XRD), field emission scanning electron microscope (FESEM), and N_2 adsorption–desorption measurement. The photocatalytic activity of the mesoporous TiO_2 nanofibers was evaluated by photocatalytic oxidation of acetone in air. The effects of hydrothermal post-treatment time on the structures and photocatalytic activity of the mesoporous TiO_2 nanofibers were discussed. The results showed that the photocatalytic activity of the TiO_2 nanofibers prepared by this method exceeded that of Degussa P25 when the hydrothermal post-treatment time was kept at 200 °C for 3–24 h. This could be attributed to the fact that the former had smaller crystallite size, larger specific surface area, and higher pore volume.

Keywords: Mesoporous; Anatase nanofibers; Photocatalytic activity; Hydrothermal post-treatment

1. Introduction

Many efforts have been devoted in recent years to developing titania semiconductor photocatalyst with highly photocatalytic activity for environmental protection procedures such as air purification, water disinfection, and hazardous water remediation due to its strong oxidizing power, chemical inertness, and nontoxicity [1–5]. It is well known that the performance of TiO_2 depends strongly on its crystallite phase, dimension, and morphology, since they give a decisive influence on the chemical and physical properties of TiO_2. One-dimensional (1D) nanostructured materials, such as nanotubes and nanofibers, are of particular significance due to their superior physicochemical properties, such as remarkable electronic, magnetic, optical, catalytic, and mechanical properties, and potential applications in environmental purification, nanodevices, gas sensors, and high-effect solar cell [6–12]. For example, several recent studies indicated that TiO_2 nanotubes possessed better properties in photocatalysis [13,14] and sensing [15], in comparison to colloidal or other forms of TiO_2. Moreover, it is expected that the combination of the 1D nanostructures and mesoporous structures would endow titania with unique properties and multiple functions. However, much attention was mainly paid to mesoporous TiO_2 particles or thin films, while 1D mesoporous TiO_2 materials were less studied, mainly due to the difficulties in fabricating such structures with good control over their dimensions [16–20]. Therefore, it is interesting to explore the synthesis of 1D nanostructured mesoporous TiO_2 materials and their photocatalytic activity.

Recently, many attempts have been made to prepare 1D TiO_2 and/or titanate nanostructured materials with large specific surface area and high pore volume [6–10,21–23]. Crystalline TiO_2 nanotubes or nanofibers were usually synthesized using porous anodic alumina as templates [16,18,19,24,25]. However, the prepared nanotubes or nanofibers by the above method generally had large diameters (>50 nm) due to the confinement of the molds used. Using a simple hydrothermal treatment of crystalline TiO_2 particles with NaOH aqueous solutions, high-quality nanotubes with uniform diameter of around 10 nm were obtained and their specific surface area reached more than 400.0 m^2/g [6,7]. Unfortunately, the obtained nanotubes showed almost no photocatalytic activity for the photocatalytic degradation of acetone in our experiment. Following the pioneering works, the nanotubes obtained by this method were actually not

* Corresponding author. Tel.: +86 27 8788 3610; fax: +86 27 8787 3610.
E-mail address: jiaguoyu@yahoo.com (J. Yu).

1010-6030/$ – see front matter © 2006 Elsevier B.V. All rights reserved.
doi:10.1016/j.jphotochem.2006.01.022

TiO_2, but might be of protonic titanate [9,26]. Considering their large specific surface area, high pore volume, and unique morphology, the obtained nanotubes will offer another possibility to design various TiO_2-related materials by post-treatment methods, such as hydrothermal post-treatment and well-controlled calcination.

Hydrothermal synthesis, a low temperature technology for materials development, was widely applied to prepare various materials due to high reactivity of reactants, easy control of solution, less air pollution, and low energy consumption under hydrothermal conditions [27]. In the present work, titanate nanotubes were first prepared by a hydrothermal reaction using a 10 M NaOH aqueous solution and Degussa P25 as precursors. Subsequently, the as-prepared nanotubes were hydrothermally post-treated at 200 °C for 1–24 h, leading to the formation of mesoporous anatase TiO_2 nanofibers. The photocatalytic activity of the mesoporous TiO_2 nanofibers was evaluated by photocatalytic oxidation of acetone in air. The effects of hydrothermal post-treatment time on the phase structure, crystallization, crystallite size, morphology, specific surface area, pore structures, and photocatalytic activity of the mesoporous TiO_2 nanofibers were discussed. This is the first report on the preparation of mesoporous anatase TiO_2 nanofibers by the hydrothermal post-treatment of the titanate nanotubes. This work may provide new insights into the preparation of mesoporous TiO_2 photocatalyst with highly photocatalytic activity.

2. Experimental

2.1. Preparation of titanate nanotubes

Titanate nanotubes were prepared using a chemical process similar to that described by Kasuga et al. [6,7] and Tian et al. [28]. TiO_2 source used for the titanate nanotubes was commercial-grade TiO_2 powder (P25, Degussa AG, Germany) with crystalline structure of ca. 20% rutile and ca. 80% anatase and primary particle size of ca. 30 nm. In a typical nanotube preparation, 1.5 g of the TiO_2 powder was mixed with 140 ml of 10 M NaOH solution, followed by hydrothermal treatment of the mixture at 150 °C in a 200 ml Teflon-lined autoclave for 48 h. After hydrothermal reaction, the precipitate was separated by filtration and washed with a 0.1 M HCl solution and distilled water until the pH value of the rinsing solution reached ca. 6.5, approaching the pH value of the distilled water. The washed samples were dried in a vacuum oven at 80 °C for 8 h.

2.2. Preparation of mesoporous TiO_2 nanofibers

In the preparation of mesoporous TiO_2 nanofibers, 0.55 g of the as-prepared titanate nanotubes were mixed with 80 ml of distilled water, followed by hydrothermal post-treatment of the mixture at 200 °C in a 100 ml Teflon-lined autoclave for 1–24 h. After the hydrothermal post-treatment, the obtained samples were filtered and dried in a vacuum oven at 80 °C for 8 h.

2.3. Characterization

Transmission electron microscopy (TEM) analyses were performed with a JEOL JEM 2010FEF electron microscope, using 200 kV accelerating voltage. The X-ray diffraction (XRD) patterns were obtained on a Bruker D8 Advance X-ray diffractometer using Cu Kα radiation at a scan rate of $0.05^\circ\ 2\theta\ s^{-1}$ and were used to determine the identity of crystalline phase and the crystallite size. The accelerating voltage and the applied current were 40 kV and 40 mA, respectively. The surface morphologies of the samples were observed using a JEOL-6700F field emission scanning electron microscope (FESEM). The thermogravimetry (TG) was performed on a TG-DTA instrument (Setaram TG-DTA 92-16, France), under a heating rate of $10\ K\ min^{-1}$ from room temperature to 1000 °C. Nitrogen adsorption–desorption isotherms were obtained on an AUTOSORB-1 (Quantachrome Instruments, USA) nitrogen adsorption apparatus. All the samples were degassed at 80 °C prior to BET measurements. The Brunauer–Emmett–Teller (BET) specific surface area (S_{BET}) was determined by a multipoint BET method using the adsorption data in the relative pressure (P/P_0) range of 0.05–0.3. The desorption isotherm was used to determine the pore size distribution using the Barret–Joyner–Halender (BJH) method [29]. The nitrogen adsorption volume at the relative pressure (P/P_0) of 0.994 was used to determine the pore volume and the average pore size.

2.4. Measurement of photocatalytic activity

Acetone (CH_3COCH_3) is a common chemical that is used extensively in various industrial and domestic applications. Therefore, we chose it as a model contaminate chemical. Photocatalytic oxidation of acetone is based on the following reaction [30–33]:

$$CH_3COCH_3 + 4O_2 \rightarrow 3CO_2 + 3H_2O \quad (1)$$

The measurement of photocatalytic activity of the mesoporous TiO_2 nanofibers was performed in a 15 L reaction reactor using the photodegradation of acetone with an initial concentration of 350 ± 20 ppm. The detailed experimental setup and process have been reported elsewhere [33]. The TiO_2 photocatalysts were prepared by coating an aqueous suspension of TiO_2 samples onto three dishes with a diameter of ca. 7.0 cm. The dishes containing catalysts were dried at 100 °C and then cooled to room temperature before being used. The weight of the TiO_2 catalysts used for each experiment was kept at ca. 0.5 g. After the catalysts were placed in the reactor, a small amount of acetone was injected with a syringe into the reactor. The reactor was connected to a $CaCl_2$-containing dryer used for controlling the initial humidity in the reactor. The acetone vapor was allowed to reach adsorption–desorption equilibrium with catalysts in the reactor prior to UV light irradiation. Integrated UV intensity in the range of 310–400 nm striking the coatings, measured with a UV radiometer (Model: UV-A, made in Photoelectric Instrument Factory of Beijing Normal University), was $2.5\ mW/cm^2$, while the peak wavelength of UV light was 365 nm. The concen-

tration analysis of acetone, carbon dioxide, and water vapor in the reactor was conducted on line with a Photoacoustic IR Multigas Monitor (INNOVA Air Tech Instruments Model 1312). The photocatalytic activity of the TiO_2 samples can be quantitatively evaluated by comparing the apparent reaction rate constants. The photocatalytic oxidation of acetone is a pseudo-first-order reaction and its kinetics may be expressed as follows: $\ln(C_0/C) = kt$ [31,32], where k is the apparent reaction rate constant, C_0 and C are the initial concentration and the reaction concentration of acetone, respectively.

3. Results and discussion

3.1. Morphology and structure of titanate nanotubes

A large amount of nanotubes with diameters of 7–12 nm and lengths of several hundreds nanometers were prepared by a hydrothermal reaction between Degussa P25 and a 10 M NaOH aqueous solution at 150 °C for 48 h (as shown in Fig. 1). EDX analysis demonstrated the absence of sodium ions in the obtained nanotubes (not shown here). Therefore, it could be concluded that the sodium ions were substituted completely by protons after the nanotubes were washed with a HCl aqueous solution and distilled water. Fig. 2 depicts the XRD patterns of P25 powder and the obtained nanotubes. The precursor P25 showed the presence of both anatase and rutile phases. After hydrothermal treatment of P25 in a 10 M NaOH solution for 48 h, the pattern of the resulted powders (nanotubes) could not correspond to anatase, rutile, brookite or their mixtures. The crystal structure of the nanotubes was similar to that of $H_2Ti_3O_7$ ($Na_2Ti_3O_7$) [8,9], $Na_xH_{2-x}Ti_3O_7$ [26], $H_xTi_{2-x/4}\square_{x/4}O_4$ ($x = 0.75$) [34], $Na_2Ti_2O_4(OH)_2$ [35], or $Na_yH_{2-y}Ti_nO_{2n+1}\cdot xH_2O$ [36], probably due to their same layered titanate family. TG curve (not shown here) showed that a mass loss of ca. 20.1% was observed in this study after the nanotubes were heated from room temperature to 1000 °C. Considering the absence of Na in the nanotubes and a large mass loss, the obtained nanotubes may be described as $H_2Ti_nO_{2n+1}\cdot xH_2O$ and can be attributed to protonic titanate.

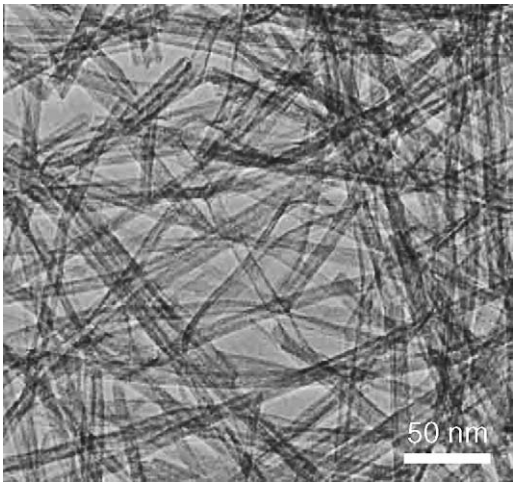

Fig. 1. TEM image of the titanate nanotubes obtained from hydrothermal treatment of P25 with NaOH solution at 150 °C for 48 h.

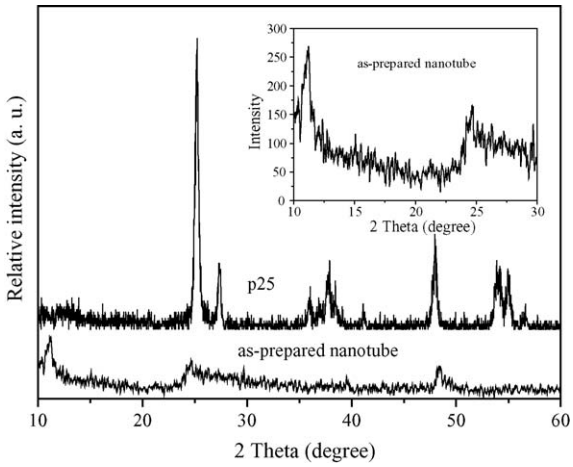

Fig. 2. XRD patterns of the raw material (P25) and the titanate nanotubes.

3.2. Phase structure and surface morphology of mesoporous TiO_2 nanofibers

Fig. 3 shows the XRD patterns of the TiO_2 nanofibers obtained by hydrothermal post-treatment of the titanate nanotubes at 200 °C for 1, 3, 7, 12, and 24 h. After hydrothermal post-treatment for 1 h, the intensity of diffraction peak located at ca. 11° (nanotubes) was weakened significantly and the anatase peak at ca. 25.5° appeared, indicating the destruction of titanate structure and the formation of anatase phase. It should be noted that the titanate and anatase TiO_2 possess some similar structure features. In titanium oxide lattice, a TiO_6 octahedron in anatase phase shares four edges with other octahedrons to form a zigzag ribbon structure [37]. In addition to the four edge-sharing TiO_6 octahedras and the zigzag ribbons structure in the titanate lattice, these zigzag ribbons then form a titanate layer by sharing the corners of these ribbons, and the protons or sodium ions can exist between the titanate layers [38]. Therefore, it seems that the anatase phase was formed by the dehydration among the layers and the rearrangement of the zigzag ribbon structures. With increasing hydrothermal post-treatment time, the diffrac-

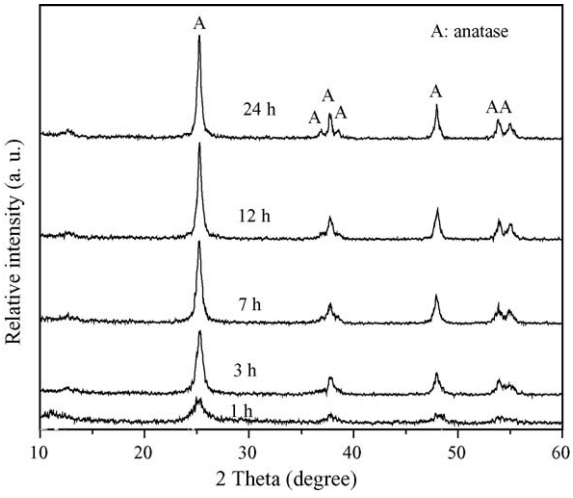

Fig. 3. XRD patterns of the TiO_2 nanofibers obtained from hydrothermal post-treatment of the titanate nanotubes at 200 °C for 1, 3, 7, 12, and 24 h.

tion peaks of the titanate nanotubes disappeared and the peaks intensities of anatase phase increased (Fig. 3), indicating the enhancement of crystallization in anatase phase. Fig. 4 shows the average crystallite size of the TiO_2 nanofibers as a function of the hydrothermal post-treatment time. With increasing hydrothermal post-treatment time, the average crystallite size increased from 8.1 to 27.3 nm due to the growth of TiO_2 crystallites. However, the crystallite size of all the TiO_2 nanofibers was smaller than that of the precursor P25 (ca. 30.0 nm).

Fig. 5 shows the SEM images of the TiO_2 nanofibers obtained by hydrothermal post-treatment of the titanate nanotubes at 200 °C for 3, 7, and 24 h. After hydrothermal post-treatment for 3 h, the TiO_2 nanofibers were observed and exhibited a diameter of 25–50 nm and a length of 0.2–3 μm (Fig. 5a and b). Meanwhile, these TiO_2 nanofibers tended to aggregate to form nanofiber bundles with diameters of 100–500 nm (Fig. 5a). Further observation indicated that the TiO_2 nanofibers were composed of many small TiO_2 particles with diameters of 15–30 nm. With increasing hydrothermal post-treatment time

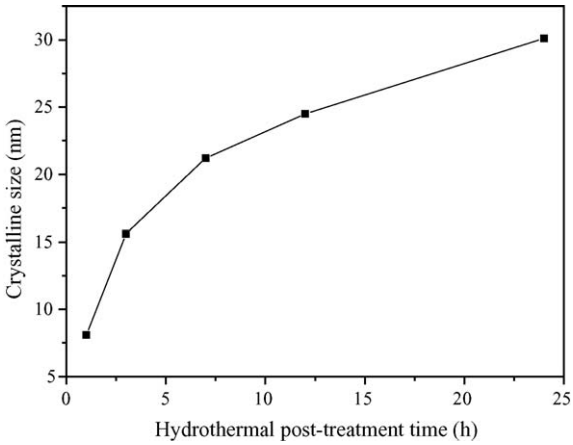

Fig. 4. Effect of hydrothermal treatment time on the crystalline size of TiO_2 nanofibers obtained from hydrothermal post-treatment of the titanate nanotubes.

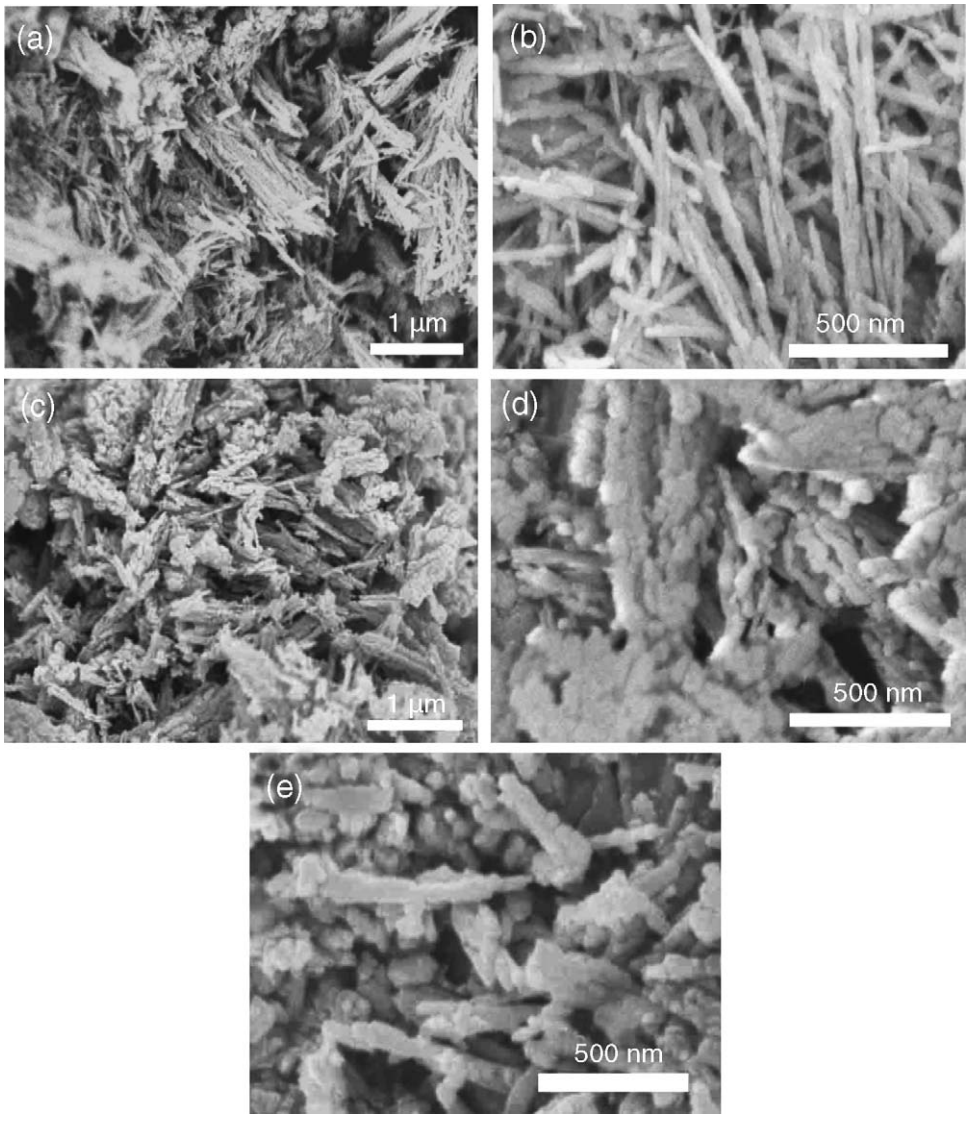

Fig. 5. SEM images of the TiO_2 nanofibers obtained from hydrothermal post-treatment of the titanate nanotubes at 200 °C for 3 h (a and b); 7 h (c and d); 24 h (e).

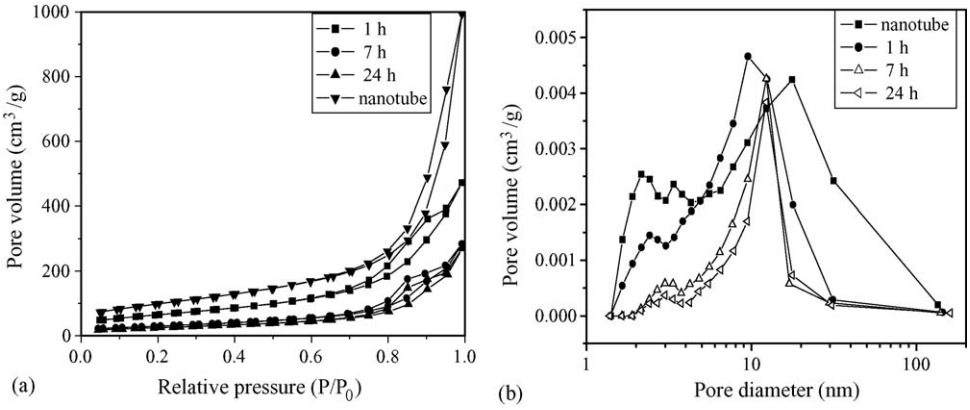

Fig. 6. Nitrogen adsorption–desorption isotherms (a) and pore-size distribution curves (b) of the TiO_2 nanofibers obtained from hydrothermal post-treatment of the titanate nanotubes at 200 °C for 0, 1, 7, and 24 h.

from 3 to 7 h, as shown in Fig. 5c and d, the length of the TiO_2 nanofibers decreased to ~2 μm, while the corresponding diameters increased to 100–500 nm which was equal to the diameters of the TiO_2 nanofiber bundles found in Fig. 5a. It seems that the hydrothermal dehydration reaction took place in the formed fiber bundlers during the hydrothermal post-treatment (3–7 h), resulting in the formation of TiO_2 fibers with larger diameters (100–500 nm). On the other hand, the larger TiO_2 fibers were composed of many TiO_2 particles with larger diameter of 25–40 nm (Fig. 5c and d) in comparison to that of TiO_2 particles found in Fig. 5b, indicating the growth of TiO_2 particles. After hydrothermal post-treatment of the titanate nanotubes at 200 °C for 24 h, the length of the TiO_2 fibers further become shorter (~800 nm) and their diameters decreased to less than 100 nm (Fig. 5e). Moreover, many TiO_2 particles with diameter of 70–150 nm were observed. It is possible that the further hydrothermal post-treatment at high-temperature (200 °C) and high-pressure conditions caused the destruction of the TiO_2 fibers and led to the formation of TiO_2 particles.

3.3. BET specific surface areas and pore structures

The nitrogen adsorption–desorption isotherms of the obtained samples are presented in Fig. 6a. All samples showed the type IV isotherms with type H3 hysteresis loops according to BDDT classification [29], indicating the presence of mesopores (2–50 nm). As for the titanate nanotubes, the observed hysteresis loops shifted to a high relative pressure $P/P_0 \approx 1$, suggesting the presence of large pores (>50 nm) [39]. Considering the morphology of the nanotubes observed in Fig. 1, the smaller pores may correspond to the pores inside the nanotubes and the diameter of these pores is equal to the inner diameter of the nanotubes, while the larger pores can be attributed to the aggregation of the nanotubes [39]. After hydrothermal post-treatment of the titanate nanotubes at 200 °C for more than 1 h, the area of the hysteresis loops at high relative pressures ($P/P_0 > 0.9$) has an obvious decrease, indicating the disappearance of some large pores (>50 nm) in the TiO_2 nanofiber samples.

Fig. 6b shows the corresponding pore size distributions of the prepared samples. The pore-size distributions of the TiO_2 nanofibers depended on the hydrothermal post-treatment time. Prior to hydrothermal post-treatment, the nanotubes exhibited a wide pore size distribution ranging from 1.5 to more than 100 nm. This was in good agreement with the previous studies though different TiO_2 sources were used as the precursors [39,40]. After hydrothermal post-treatment of the titanate nanotubes at 200 °C for 1 h, the pore size distribution of the sample become narrower (1.5–30 nm) and the larger pores (>30 nm) almost disappeared. With further increase in the hydrothermal post-treatment time, the pore size distribution range of the TiO_2 nanofibers become further smaller, while the average pore diameter increased from 12.4 to 18.5 nm due to the growth of TiO_2 crystallites (Fig. 3). Meanwhile, the pore volume of mesopores located at 1.5–10 nm decreased significantly. This may be attributed to the collapse of the tube structure in the nanotubes during the hydrothermal post-treatment. Textural parameters derived from the nitrogen adsorption–desorption isotherm data are summarized in Table 1. When P25 was transformed into the titanate nanotubes, there was a significant increase for S_{BET} from 60.0 to 355.7 m^2/g and for pore volume from 0.06 to 1.54 cm^3/g due to the formation of nanotube structures. As for the TiO_2 nanofibers, with increasing post-treatment time from 1 to 7 h, the S_{BET} and pore volume of the samples decreased obviously to 108.2 m^2/g and 0.44 cm^3/g, respectively. According to the above analysis of the pore size distribution curves in Fig. 6b,

Table 1
Textural parameters derived from the nitrogen adsorption–desorption isotherm data

Samples	S_{BET} (m^2/g)[a]	Pore volume (cm^3/g)[b]	Average pore size (nm)[b]
P25	60.0	0.06	3.8
Nanotubes	355.7	1.54	17.3
1 h	235.4	0.73	12.4
7 h	108.2	0.44	16.2
24 h	90.2	0.42	18.5

[a] The BET specific surface area was determined by multipoint BET method suing the adsorption data in the relative pressure (P/P_0) range of 0.05–0.3.

[b] Pore volume and average pore size were determined by nitrogen adsorption volume at the relative pressure of 0.994.

the decrease of the S_{BET} was mainly attributed to the collapse of the tube structure and the growth of TiO_2 crystallites, while the obvious decline in the pore volume was attributed to the disappearance of larger pore (>30 nm) and the destruction of nanotube structures. With further increase in the hydrothermal post-treatment time from 7 to 24 h, the specific surface area and pore volume of the samples showed a further decrease. The decreasing value was 18.0 m^2/g for S_{BET} and 0.02 cm^3/g for pore volume, which mainly resulted from the further growth of TiO_2 crystallites (Fig. 3). However, the S_{BET} (>90.0 m^2/g) and pore volume (>0.40 cm^3/g) for the obtained TiO_2 nanofibers by this method were obviously larger than those of P25. The high specific surface area and pore volume of the samples are expected to have a wider application in photocatalysis, selective adsorption, ultraviolet blockers, separation, sensing, and as functional filling materials in textile, paints, paper, and cosmetics.

3.4. Photocatalytic activity

The photocatalytic activity of the mesoporous TiO_2 nanofibers was evaluated by photocatalytic oxidation of acetone in air. Fig. 7 shows the concentration change of acetone and carbon dioxide with UV illumination time. It could be seen that the concentration of the produced carbon dioxide was about three times higher than that of the destroyed acetone. Further observations indicated that the concentration of acetone and carbon dioxide changed linearly with increasing illumination time, indicating the complete decomposition of acetone [41].

The degradation rate constant (or apparent rate constant) of acetone was used to characterize the photocatalytic activity of the mesoporous TiO_2 nanofibers. Fig. 8 shows the dependence of apparent rate constants (k, min^{-1}) of the TiO_2 nanofibers on the hydrothermal post-treatment time at 200 °C. For comparison, the photocatalytic activity of commercial photocatalyst P25 was also tested under identical conditions. Prior to hydrothermal post-treatment, the titanate nanotubes exhibited no photocatalytic activity for the photocatalytic degradation of acetone in air. After hydrothermal post-treatment of the titanate nanotubes at 200 °C for 1 h, the sample exhibited a decent photocatalytic activity due to the formation of anatase phase. With increasing

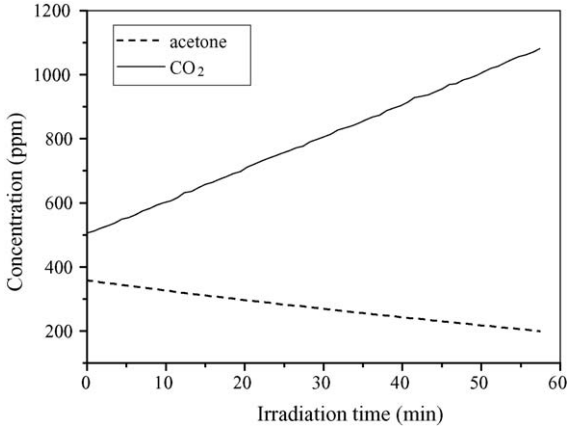

Fig. 7. Concentration change of acetone and carbon dioxide with UV illumination time.

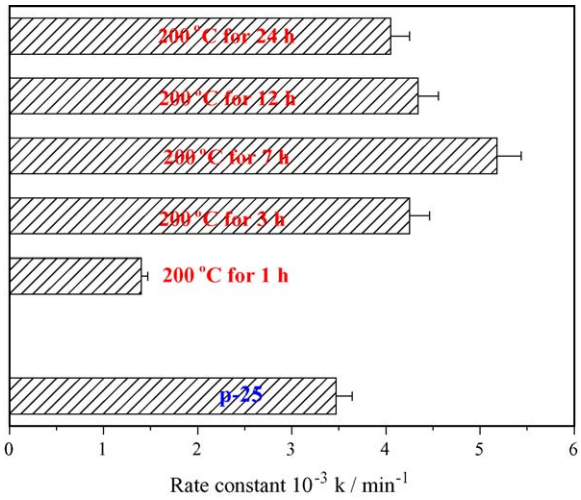

Fig. 8. The dependence of apparent rate constants of the TiO_2 nanofibers on the hydrothermal post-treatment time.

hydrothermal post-treatment time from 1 to 7 h, the k increased significantly and reached a maximum value of 5.18×10^{-3} at 7 h. This was due to the fact that the TiO_2 nanofibers showed better crystallization in anatase phase. With further increase in the hydrothermal post-treatment time, the photocatalytic activity of the samples decreased owing to the decrease of the S_{BET} and pore volume (Table 1). However, as for the TiO_2 nanofibers obtained by hydrothermal post-treatment of the titanate nanotubes at 200 °C for 3–24 h, the samples showed a higher photocatalytic activity than that of P25. The k was determined to be 3.47×10^{-3} for Degussa P25, which is well known to have good photocatalytic activity. The superior activity of TiO_2 nanofibers may be ascribed to the fact that the former has larger specific surface area, smaller crystallite size, and higher pore volume. Large specific surface area allows more gaseous reactants to be absorbed onto the surface of the photocatalyst, while high pore volume (mesopores) allows rapid diffusion of various gaseous products during the photocatalytic reaction, which can enhance the rate of photocatalytic reaction. Furthermore, compared with nanosized TiO_2 powder photocatalyst, such as P25, TiO_2 nanofiber photocatalyst can be readily separated from the water in a slurry system after photocatalytic reaction because their lengths are at a scale of several micrometers. Therefore, the obtained TiO_2 nanofiber photocatalyst may be suitable for the application at an industrial scale [42].

4. Conclusions

Mesoporous anatase TiO_2 nanofibers with highly photocatalytic activity were prepared by a simple hydrothermal post-treatment of titanate nanotubes. Hydrothermal post-treatment at 200 °C resulted in the destruction of nanotube structures and the formation of anatase TiO_2 nanofibers. The hydrothermal post-treatment time has an obvious effect on the crystallization, crystallite size, morphology, specific surface area, pore structures and photocatalytic activity of the mesoporous TiO_2 nanofibers. With increasing hydrothermal post-treatment time, the special surface area and pore volume decreased due to the growth of

TiO_2 crystallites. However, the resulted TiO_2 nanofibers could partially maintain the advantage of high specific surface area and pore volume of titanate nanotubes. The photocatalytic activity of the TiO_2 nanofibers prepared by this method exceeded that of Degussa P25 when the titanate nanotubes were hydrothermally post-treated at 200 °C for 3–24 h. This can be attributed to the fact that the former had larger specific surface area, smaller crystallite size, and higher pore volume.

Acknowledgements

This work was partially supported by the National Natural Science Foundation of China (50272049 and 20473059). This work was also financially supported by the Excellent Young Teachers Program of MOE of China and Project-Sponsored by SRF for ROCS of SEM of China.

References

[1] K. Honda, A. Fujishima, Nature 238 (1972) 37.
[2] M.R. Hoffmann, S.T. Martin, W. Choi, D.W. Bahnemann, Chem. Rev. 95 (1995) 69.
[3] F.B. Li, X.Z. Li, M.F. Hou, Appl. Catal. B 48 (2004) 185.
[4] J.C. Zhao, T.X. Wu, K.Q. Wu, K. Oikawa, H. Hidaka, N. Serpone, Environ. Sci. Technol. 32 (1998) 2394.
[5] J.G. Yu, H.G. Yu, B. Cheng, X.J. Zhao, J.C. Yu, W.K. Ho, J. Phys. Chem. B 107 (2003) 13871.
[6] T. Kasuga, M. Hiramatsu, A. Hoson, T. Sekino, K. Niihara, Langmuir 14 (1998) 3160.
[7] T. Kasuga, M. Hiramatsu, A. Hoson, T. Sekino, K. Niihara, Adv. Mater. 11 (1999) 1307.
[8] Q. Chen, W.Z. Zhou, G.H. Du, L.M. Peng, Adv. Mater. 14 (2002) 1208.
[9] G.H. Du, Q. Chen, R.C. Che, Z.Y. Yuan, L.P. Peng, Appl. Phys. Lett. 79 (2001) 3702.
[10] B.D. Yao, Y.F. Chan, X.Y. Zhang, W.F. Zhang, Z.Y. Yang, N. Wang, Appl. Phys. Lett. 82 (2003) 281.
[11] Z.Y. Yuan, W. Zhou, B.L. Su, Chem. Commun. (2002) 1202.
[12] J.G. Yu, J.C. Yu, W.K. Ho, L. Wu, X.C. Wang, J. Am. Chem. Soc. 126 (2004) 3422.
[13] D.Y. Zhang, L.M. Qi, Chem. Commun. (2005) 2735.
[14] S.Z. Chu, S. Inoue, K. Wada, D. Li, H. Haneda, S. Awatsu, J. Phys. Chem. B 107 (2003) 6586.
[15] O.K. Varghese, D.W. Gong, M. Paulose, K.G. Ong, E.C. Dickey, C.A. Grimes, Adv. Mater. 15 (2003) 624.
[16] P. Hoyer, Langmuir 12 (1996) 1411.
[17] B.B. Lakshmi, P.K. Dorhout, C.R. Martin, Chem. Mater. 9 (1997) 857.
[18] S.M. Liu, L.M. Gan, L.H. Liu, W.D. Zhang, H.C. Zeng, Chem. Mater. 14 (2002) 1391.
[19] S. Lee, C. Jeon, Y. Park, Chem. Mater. 16 (2004) 4292.
[20] M.S. Sander, M.J. Cote, W. Gu, B.M. Kile, C.P. Tripp, Adv. Mater. 16 (2004) 2052.
[21] Y.Q. Wang, G.Q. Hu, X.F. Duan, H.L. Sun, Q.K. Xue, Chem. Phys. Lett. 365 (2002) 427.
[22] Q.H. Zhang, L. Gao, J. Sun, S. Zheng, Chem. Lett. (2002) 226.
[23] R. Ma, Y. Bando, T. Sasaki, J. Phys. Chem. B 108 (2004) 2115.
[24] H. Imai, Y. Takei, K. Shimizu, M. Matsuda, H. Hirashima, J. Mater. Chem. 9 (1999) 2971.
[25] Y. Lei, L.D. Zhang, G.W. Meng, G.H. Li, X.Y. Zhang, C.H. Liang, W. Chen, S.X. Wang, Appl. Phys. Lett. 78 (2001) 1125.
[26] X.M. Sun, Y.D. Li, Chem. Eur. J. 9 (2003) 2229.
[27] S.H. Feng, R.R. Xu, Acc. Chem. Res. 34 (2001) 239.
[28] Z.R. Tian, J.A. Voigt, J. Liu, B. Mckenzie, H. Xu, J. Am. Chem. Soc. 125 (2003) 12384.
[29] K.S.W. Sing, D.H. Everett, R.A.W. Haul, L. Moscou, R.A. Pierotti, J. Rouquerol, T. Siemieniewska, Pure Appl. Chem. 57 (1985) 603.
[30] M.E. Zorn, D.T. Tompkins, W.A. Zeltner, M.A. Anderson, Appl. Catal. B: Environ. 23 (1999) 1.
[31] J.G. Yu, J.C. Yu, M.K.P. Leung, W.K. Ho, B. Cheng, X.J. Zhao, J.C. Zhao, J. Catal. 217 (2003) 69.
[32] J.C. Yu, J.G. Yu, W.K. Ho, Z.T. Jiang, L.Z. Zhang, Chem. Mater. 14 (2002) 3808.
[33] J.G. Yu, M.H. Zhou, B. Cheng, H.G. Yu, X.J. Zhao, J. Mol. Catal. A 227 (2005) 75.
[34] R. Ma, Y. Bando, T. Sasaki, Chem. Phys. Lett. 380 (2003) 577.
[35] J.J. Yang, Z.S. Jin, X.D. Wang, W. Li, J.W. Zhang, S.L. Zhang, Dalton Trans. (2003) 3898.
[36] J. Canales, P.G. Bruce, Angew. Chem. Int. Ed. 43 (2004) 2286.
[37] H. Izawa, S. Kikkawa, M. Koizumi, J. Phys. Chem. 86 (1982) 5023.
[38] H.Y. Zhu, Y. Lan, X.P. Gao, S.P. Ringer, Z.F. Zheng, D.Y. Song, J.C. Zhao, J. Am. Chem. Soc. 127 (2005) 6730.
[39] D.V. Bavykin, V.N. Parmon, A.A. Lapkin, F.C. Walsh, J. Mater. Chem. 14 (2004) 3370.
[40] C.C. Tsai, H. Teng, Chem. Mater. 16 (2004) 4352.
[41] J.C. Yu, L.Z. Zhang, J.G. Yu, Chem. Mater. 14 (2002) 4647.
[42] H. Zhu, X. Gao, Y. Lan, D. Song, Y. Xi, J. Zhao, J. Am. Chem. Soc. 126 (2004) 8380.